Investigation of the effects of flow conditions at rotor inlet on mixed flow turbine performance for automotive applications

Morrison, R., Spence, S., Kim, S., Filsinger, D., & Leonard, T. (2016). Investigation of the effects of flow conditions at rotor inlet on mixed flow turbine performance for automotive applications. Paper presented at International Turbocharging Seminar 2016, Tianjin, China.

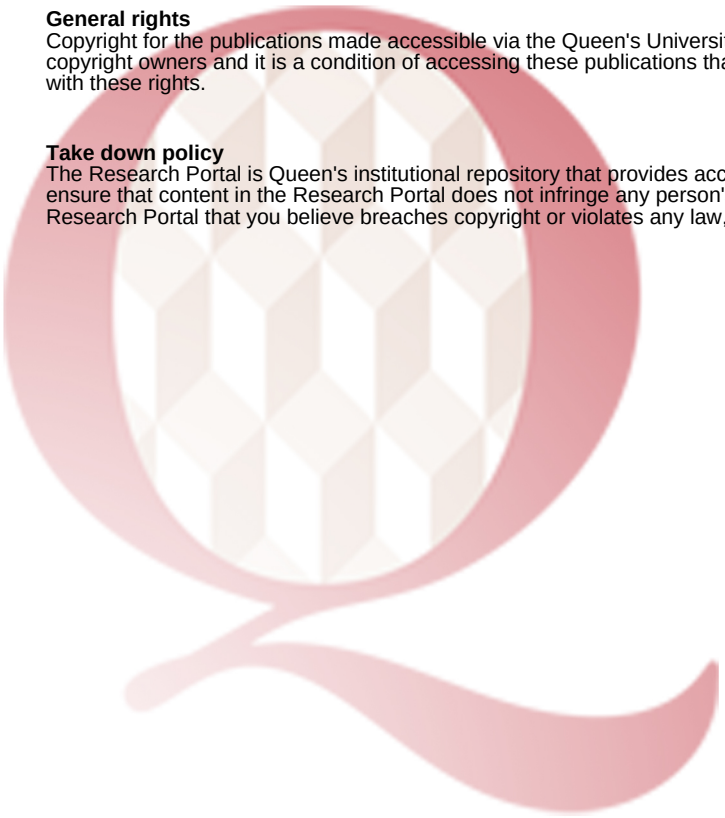

Investigation of the Effects of Flow Conditions at Rotor Inlet on Mixed Flow Turbine Performance for Automotive Applications.

Richard Morrison[1*], Stephen Spence [1], Sung In Kim [1], Dietmar Filsinger [2], Thomas Leonard [2]

[1] *Queens University Belfast, Belfast, United Kingdom*
[2] *IHI Charging Systems International, Heidelberg, Germany*

**corresponding author: Tel.:+44-28-90974569;*
E-mail rmorrison13@qub.ac.uk

Abstract

Current trends in the automotive industry have placed increased importance on engine downsizing for passenger vehicles. Engine downsizing often results in reduced power output and turbochargers have been relied upon to restore the power output and maintain drivability. As improved power output is required across a wide range of engine operating conditions, it is necessary for the turbocharger to operate effectively at both design and off-design conditions. One off-design condition of considerable importance for turbocharger turbines is low velocity ratio operation, which refers to the combination of high exhaust gas velocity and low turbine rotational speed. Conventional radial flow turbines are constrained to achieve peak efficiency at the relatively high velocity ratio of 0.7, due the requirement to maintain a zero inlet blade angle for structural reasons. Several methods exist to potentially shift turbine peak efficiency to lower velocity ratios. One method is to utilize a mixed flow turbine as an alternative to a radial flow turbine. In addition to radial and circumferential components, the flow entering a mixed flow turbine also has an axial component. This allows the flow to experience a non-zero inlet blade angle, potentially shifting peak efficiency to a lower velocity ratio when compared to an equivalent radial flow turbine.

This study examined the effects of varying the flow conditions at the inlet to a mixed flow turbine and evaluated the subsequent impact on performance. The primary parameters examined were average inlet flow angle, the spanwise distribution of flow angle across the inlet and inlet flow cone angle. The results have indicated that the inlet flow angle significantly influenced the degree of reaction across the rotor and the turbine efficiency. The rotor studied was a custom in-house design based on a state-of-the-art radial flow turbine design. A numerical approach was used as the basis for this investigation and the numerical model has been validated against experimental data obtained from the cold flow turbine test rig at Queen's University Belfast. The results of the study have provided a useful insight into how the flow conditions at rotor inlet influence the performance of a mixed flow turbine.

1. Introduction

Engine downsizing has become an important factor for improving vehicle performance in the automotive sector. Engine downsizing refers to a reduction in engine capacity, allowing for a lower engine mass and ultimately a mass reduction throughout the entire vehicle. Smaller capacity spark ignition engines can be expected to have lower throttling losses at part load conditions, compared to their larger counterparts. A consequence of engine downsizing is a reduction in power output due to the smaller swept volume, which can have an adverse impact on vehicle drivability. A common technique to improve the power output is to provide forced induction by means of a turbocharger [1]. Downsizing combined with turbocharging can be advantageous to automotive engine performance as it often shifts the region of minimum specific fuel consumption to lower engine speeds and torque outputs. This is beneficial for urban driving conditions. Additionally, turbocharging can increase engine power output without increasing mechanical losses [2]. The turbocharger unit is driven by the expansion of exhaust gas through a turbine. To ensure rapid response to transient driving events, it is crucial to have a turbocharger rotating assembly with minimal inertia and high turbine efficiency. Conventional turbochargers employ radial flow turbines (RFT) and optimum performance is achieved for a compromise between competing factors, including turbine efficiency and rotational inertia.

2. Technology review

A key factor for determining turbine efficiency is the relative difference between the blade angle and the flow angle at the blade leading edge, termed the incidence angle. The incidence angle can be considered positive when the relative flow velocity is impinging upon the pressure side of the blade, and negative when it impinges upon the suction side of the blade. When the incidence angle is excessively positive or negative flow separation occurs on the blade suction or pressure surfaces, respectively. Several previous studies have concluded that peak efficiency for a radial flow turbine is achieved with a modest negative incidence angle. The ideal range has been quoted as -20° to -30° [3] or even as high as -40° [4]. Spence and Artt [5] conducted an experimental assessment of incidence losses in a RFT and found that for a small stator area and mass flow rate the turbine was reasonably insensitive to incidence angles between -40° and +40°. As the stator area and mass flow rate were increased, the rotor became less tolerant of positive incidence angle and peak efficiency occurred for incidence angles between -20° and -40°. At the optimum incidence

range, the rotor was tolerant to changes of up to 10° without a significant drop in efficiency. Although it may appear intuitive that optimum efficiency would be achieved with flow parallel to the blade at inlet, representing zero incidence, this is not the case. Within the blade passage there is strong movement of flow towards the pressure surface from the suction surface due to the positive shift in the velocity vector resulting from the blade speed reducing more rapidly than the tangential flow velocity [6], establishing a relative eddy within the radial portion of the blade passage. A negative incidence angle acts to offset this effect.

As the incidence angle is dependant in part on the flow and blade velocities, it is closely connected to the velocity ratio (U/C_s) parameter, which represents the relationship between blade tip velocity and flow isentropic sprouting velocity. This is an important parameter for defining turbine operating conditions. For radial flow turbines, peak efficiency is typically achieved at the relatively high velocity ratio of 0.7, which corresponds to a negative incidence angle [3]. This is undesirable for current automotive applications where high turbine efficiency is required for a wide range of engine operating conditions, shifting the focus for turbine design to off-design operation and low velocity ratio performance. At low velocity ratio operation turbine performance is often compromised by excessive positive incidence angles. The incidence angle can be reduced by including a non-zero inlet blade angle. Walkingshaw et al demonstrated that this was possible by implementing a non-zero inlet blade angle in prototype rotors [7]. The drawback of using a non-zero inlet blade angle in radial turbine design is an increase in blade stress due to the interruption of the radial fibres of the blade and the associated bending.

An alternative means to achieve a non-zero inlet blade angle is to use a mixed flow turbine (MFT), which have the potential to achieve peak efficiency at lower velocity ratios than a conventional RFT [8]. A study by Lüddecke et al. [9] provided experimental evidence that optimum efficiency for a MFT can be achieved at a velocity ratio below that of an equivalent RFT. This characteristic was attributed to the improved inlet blade angle, swallowing capacity and rotational inertia of the MFT. To date, MFT rotors have been successfully incorporated into turbochargers for gasoline automotive engines, as documented in [10-13].

The flow at the inlet to a mixed flow turbine has both radial and axial components in the meridional plane, producing a non-90° flow cone angle (λ). The blade angle (β_b) experienced by the flow is dependent on the flow cone angle and blade camber angle (ϕ), and is calculated using equation 1, with the angle definitions provided in Figure 1. Therefore, by including a non-90° flow cone angle, a non-zero blade angle can be achieved without compromising the structural integrity of the blade. The incidence angle for a mixed flow turbine is calculated by subtracting β_b from the flow angle, where flow angle is defined as the angle of the flow taken from the meridional direction in the plane of the flow cone angle.

A study by Palfreyman and Martinez-Botas [14] compared flow features in typical RFT and MFT rotors and observed that the primary loss structures varied between the turbine types. The RFT experienced significant entropy generation in the region close to the shroud, attributed to severe turning of the flow in the meridional direction. However, the MFT experienced large entropy generation as a result of the positive incidence close to the hub. The incidence angle increased towards the hub due to the non-constant radius of the leading edge. As the radius decreased towards the hub, blade speed reduced and circumferential flow velocity increased, due to the conservation of angular momentum. This created an increase in positive incidence across the span of the leading edge from the shroud to the hub [14].

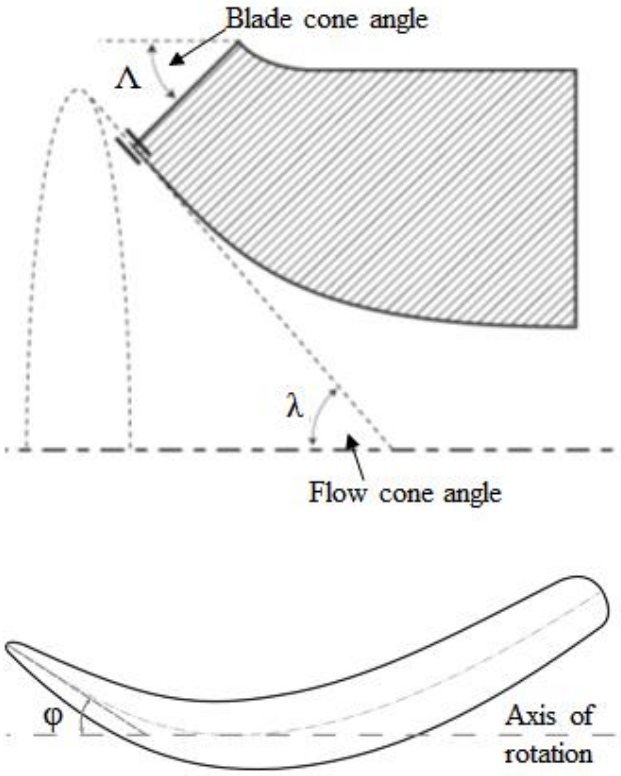

Figure 1 - Flow cone angle, λ, blade cone angle, Λ (top) [15] and blade inlet camber angle, φ (bottom)

$$tan\beta_b = cos\lambda \tan\phi \quad (1)$$

An important parameter of turbine design is the degree of reaction across the rotor. This is the ratio of static enthalpy change across the rotor to the static enthalpy change across the complete stage, and is defined by Equation 2. A small degree of reaction indicates relatively little enthalpy drop and flow acceleration across the rotor, whereas a higher reaction infers greater enthalpy drop and flow acceleration [6]. A reaction of 50% implies equal enthalpy drop in both the stator and the rotor. The advantages of low reaction turbines include a reduction of tip leakage flow and higher stage loading. However a degree of reaction below 10% can result in a drop in efficiency, even for low reaction turbines [16]. At 50% reaction the turbine has the advantage of reduced

losses due to the high flow acceleration and improved performance over a range of operating conditions [17]. Shapiro et al., as cited in [18], conducted an evaluation of two dimensional blading efficiency. The work revealed that for a stage loading value of unity, peak efficiency was achieved for a degree of reaction of 50%. However, for a stage loading of two or greater, total-to-static efficiency increased as the reaction decreased.

$$R = \frac{h_2 - h_3}{h_1 - h_3} \quad (2)$$

3. Methodology

The numerical study was undertaken using the ANSYS-CFX computational fluid dynamics (CFD) software package. A single blade passage was simulated to improve computational efficiency, reducing the time required per simulation. This approach also allowed for validation of the results using the cold flow test rig at Queen's University Belfast (QUB), which produced an axis-symmetric flow field at the inlet to the turbine. The test rig was equipped with pre-swirl vanes to create levels of swirl equivalent to what is typically produced by a turbocharger turbine housing. Additionally, by adopting this approach any asymmetric flow field effects generated by a volute tongue were not present. The rotor selected for the study was a non-commercial MFT design developed as part of a previous study at QUB and was derived from a state-of-the-art radial flow turbine [15]. The rotor consisted of 9 blades, with λ = 30° and an idealised β_b = 30°. A typical turbocharger turbine is not equipped with a diffuser, however, for this study a diffuser was included to accurately represent the QUB cold flow turbine test rig. The rotor and diffuser were modelled as a single domain, with the diffuser shroud defined as a counter rotating wall to account for its stationary position; this avoided any distorting effect from an interface just downstream of the rotor trailing edges. The outlet flow properties were extracted from the model at a location one radius downstream of the trailing edge, to negate the effects of the diffuser. The shear stress transport (SST) turbulence model was selected for the simulations as it has been demonstrated to achieve good agreement with experimental validation in previous studies at QUB [19].

The numerical model was deemed to have achieved sufficient convergence when a steady state had been achieved for selected quantities and the root-mean-squared (RMS) residuals were below 1e-4, although most simulations achieved RMS residuals below 1e-5. All numerical simulations were conducted using the High Performance Computing facilities at QUB. Four different mesh densities were examined for the grid sensitivity study. Each mesh was created using the ANSYS TurboGrid software and the density varied from one million to four million nodes. The y+ values for all wall boundaries was maintained below eleven for the study, with the majority below the recommended value of three. The parameters the meshes were evaluated for were overall efficiency and mass flow rate as well as outlet profiles of velocity, static entropy and pressure, amongst over criteria. A mesh with two million nodes was deemed suitably grid independent for the study. To ensure the tip leakage flow was accurately captured, the mesh contained 28 cells across the tip gap. Simulations of the turbine with the pre-swirl vanes were conducted at a number of different operating conditions. A meridional outline of the computational domain is provided in Figure 2. The simulation results were validated against experimental test data for the rotor. The numerical results showed good agreement with the experimental results, illustrated in Figure 3, with a maximum efficiency difference of 1.6% at the off-design condition. The numerical model was deemed sufficiently validated for the study.

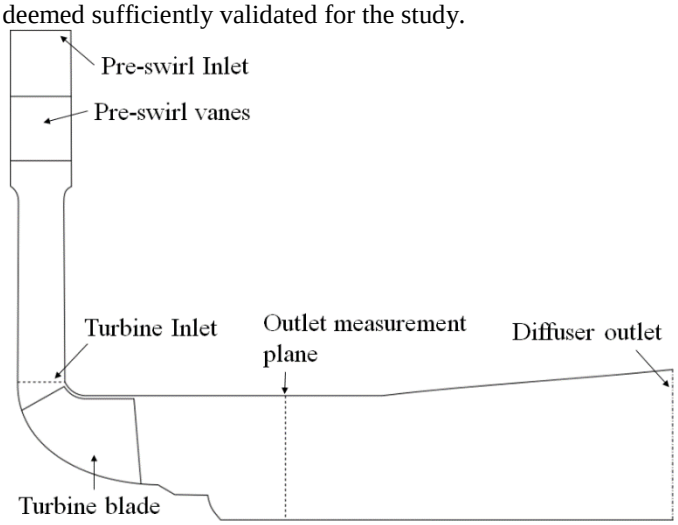

Figure 2 - Meridional view of computational domain

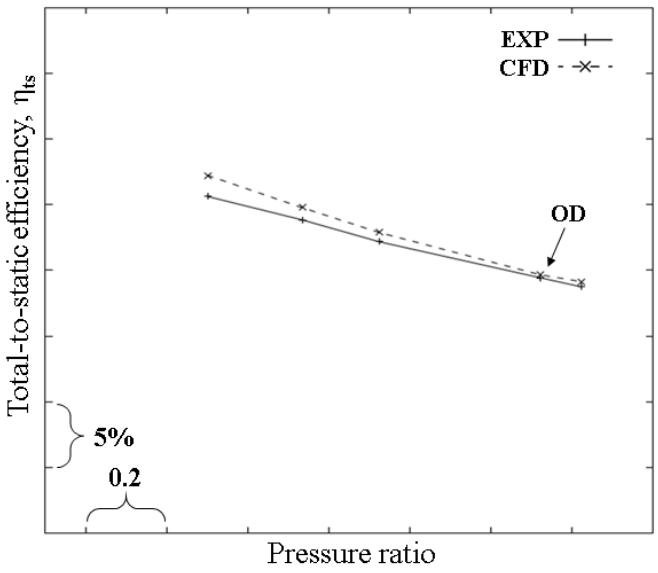

Figure 3 - Comparison of numerical and experimental results, with the off-design condition (OD) highlighted

To allow for the effects of different inlet flow conditions to be effectively evaluated, the pre-swirl vanes were removed from the simulation and boundary conditions were imposed at the inlet to the rotor passage. This allowed for the inlet flow angle to be easily controlled. Two operating points were selected for the study, one close to the design condition, and one corresponding to off-design operation. The design point represented a high rotor speed and a moderate pressure ratio, with a velocity ratio close to the optimum and was typified by

negative incidence. The off-design point corresponded to a 45% reduction in rotational speed and 10% increase in pressure ratio compared to the design condition. This produced a low velocity ratio and is typified by strong positive incidence. The total pressure at rotor inlet for each case was determined from the full domain simulations, which included the pre-swirl vanes.

The initial stage of the study involved determining the optimum inlet flow angle based on uniform flow conditions in both the circumferential and spanwise directions. To provide consistency, the same total pressure was used for each case. In practice, the total pressure may vary between cases due to changes in loss associated with generating the different rotor inlet flow angles. Imposing a uniform inlet flow angle produced idealised flow conditions, as loss generating features typically created by upstream components, were not present. This allowed for improved analysis of the impact of inlet flow angle, as the effects were not masked by secondary flow features.

After the initial stage of the study was completed the inlet flow angle that produced peak efficiency was selected as the baseline for the second stage. The second stage of the study focused on examining the effects of changing the flow angle across the span of the inlet. To achieve a valid comparison between cases, it was deemed necessary to ensure approximately equal mass flow rates for each spanwise flow angle distribution. From a one dimensional perspective, this meant maintaining approximately the same average radial velocity across the inlet for each case. To achieve this while maintaining the constant total pressure criteria, the average inlet flow angle was kept constant. This ensured the average inlet radial velocity remained constant and, therefore, the mass flow rate. Several different profiles were created that varied the flow angle in the spanwise direction while still maintaining the same average angle.

4. Results and discussion

4.1 Effects of inlet flow angle

The angle of the flow as it enters the rotor passage is perhaps one of the most influential parameters for turbine performance. It is also a parameter that the turbine designer has a reasonable level of control over, as inlet flow angle is dependent on volute A/R ratio and channel width. Therefore, it is important when defining A/R ratio that the designer has a comprehensive understanding of the impact of altering the inlet flow angle.

The turbine was analysed for a range of different flow angles and a comparison of turbine total-to-total efficiency in relation to the relative inlet flow angle is provided in Figure 4 and in relation to incidence angle in Figure 5. At the design condition the optimum incidence angle range was determined to be between -15° and +20°. This represents a shift in the positive direction compared to what would be typically expected for a RFT. This is due to the lower inlet to outlet radius ratio for a MFT, reducing the extent of the Coriolis Effect and strength of the relative eddy that must be overcome. For the off-design condition the optimum range shifted in the positive direction to between +15° and +30°. The results implied that the optimum incidence angle for the turbine is dependent on operating condition.

Three off-design cases were selected for detailed analysis. The cases represented the optimum incidence angle, i=30°, excessively positive incidence, i=44°, and an incidence angle below the optimum, i=2°. Both the i=44° and i=2° cases had approximately equal efficiency. A comparison of the spanwise distribution of incidence angle at rotor leading edge for the three selected cases is provided in Figure 6. The distribution of incidence angle across the span is typical of what would be expected for a MFT, with incidence becoming increasingly positive towards the hub due to the effects of decreasing radius.

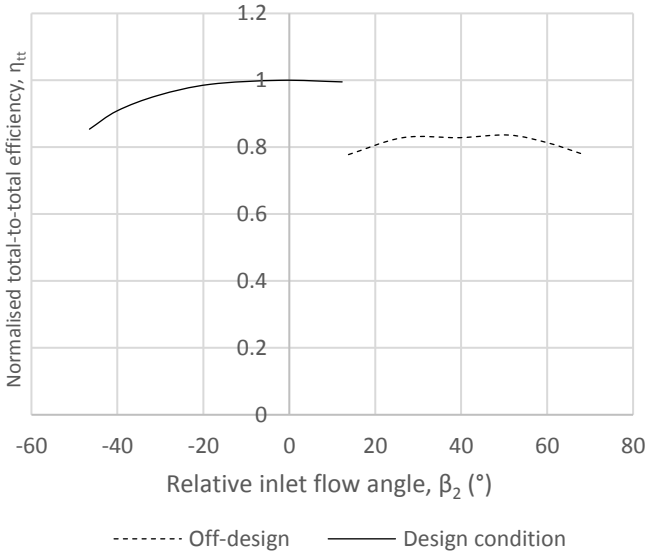

Figure 4 – Normalised total-to-total efficiency vs relative flow angle at the domain inlet

The rotor included a non-constant blade camber angle across the span. The blade camber angle increased from shroud to the hub to counteract the effects of decreasing radius. However, the blade camber angle could not be sufficiently increased to completely negate the effects. The smaller blade camber angle close to the shroud was a contributing factor to the more positive incidence in this region. The level of incidence experienced in the i=2° case created little flow separation across the leading edge, except for small portion close to the tip gap. Both cases i=30° and i=44° experienced suction surface separation across the leading edge, caused by positive incidence, illustrated in Figure 7. For the i=44° case the separated region was significant and occupied a large portion of the flow passage, blocking up to 37% of the passage at 40% chord, as illustrated in Figure 9.

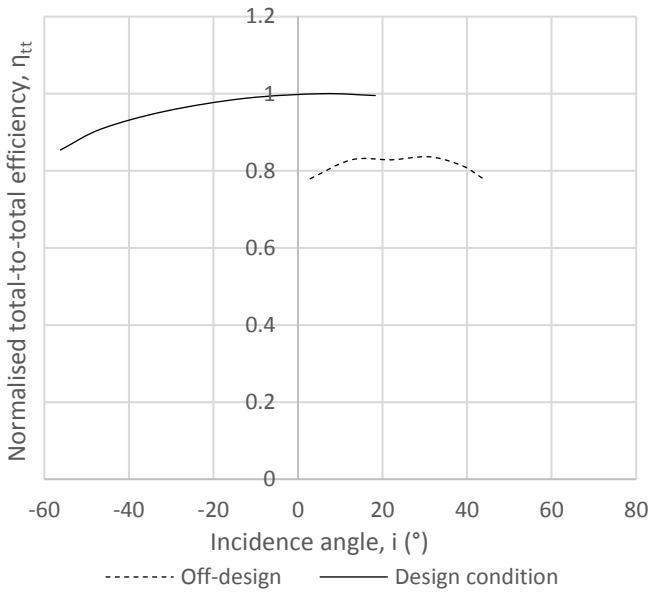

Figure 5 – Normalised total-to-total efficiency vs incidence angle at rotor leading edge

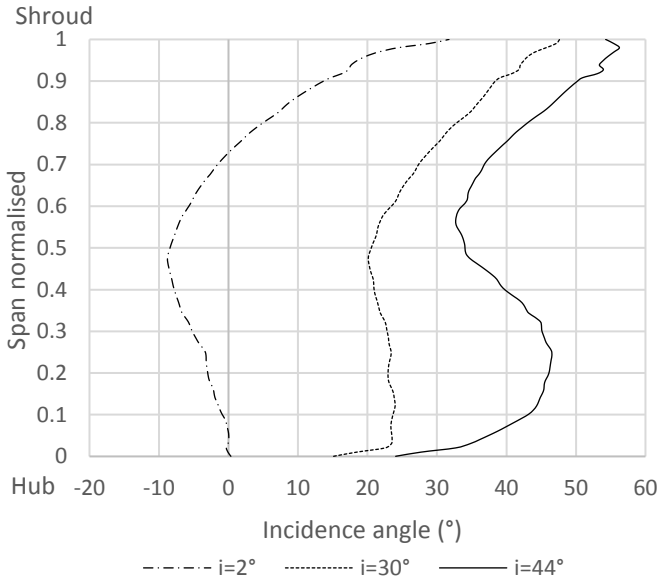

Figure 6 - Spanwise distribution of incidence angle for off-design cases

To calculate degree of reaction it is necessary to know the conditions at inlet for the pre-swirl vane, which was not present for this analysis. The assumption was therefore made that there would be minimal flow acceleration though the pre-swirl vane and the temperature at pre-swirl vane inlet would equal the total temperature imposed at inlet to the rotor passage. For the cases examined the degree of reaction was calculated as 0.03, 0.20 and 0.45 for cases i=44°, i=20° and i=2° respectively. The degree of reaction increased as incidence angle decreased due to the flow undergoing less turning in the rotor passage. This corresponded to greater flow acceleration in the rotor passage for the low incidence angle cases.

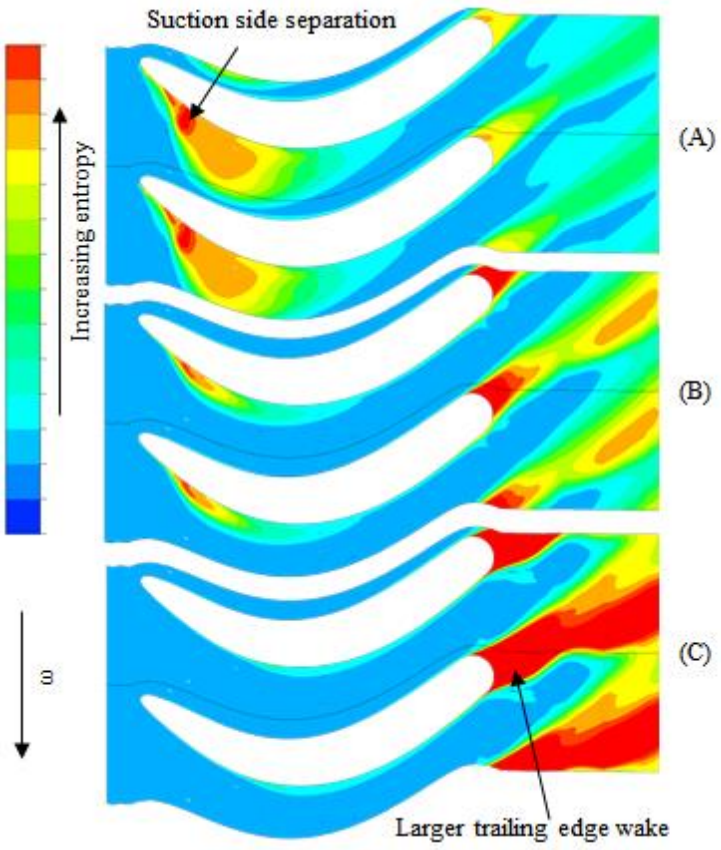

Figure 7 - Static entropy plots for off-design cases i=44° (A), i=30° (B) and i=2° (C) at 10% span

In spite of the lower level of positive incidence, overall blade loading was highest for the i=2° case. Although higher blade loading typically produces greater work output from the blade, it can result in additional losses within the rotor passage. A comparison of blade loading for the three cases at 90% span is provided in Figure 8. Downstream of 15% chord position, the blade loading of the i=2° case significantly exceeded that of the other cases. This corresponded with the increased tip leakage flow, which produced strong leakage vortices, lowering the turbine efficiency for the i=2° case. Compared to the i=30° case, the i=2° case experienced 14% higher circumferential flow velocity through the tip gap, whereas the i=44° case had a reduction of 22%.

Compared to the other cases, the i=2° case experienced higher blade loading from 15% chord to the trailing edge. The greater blade loading, and thus pressure difference, at the trailing edge resulted in a larger trailing edge wake with higher intensity, as highlighted in Figure 7. It should be noted that this discussion represents a highly off-design operating condition and consequently a flow field that is far from optimal.

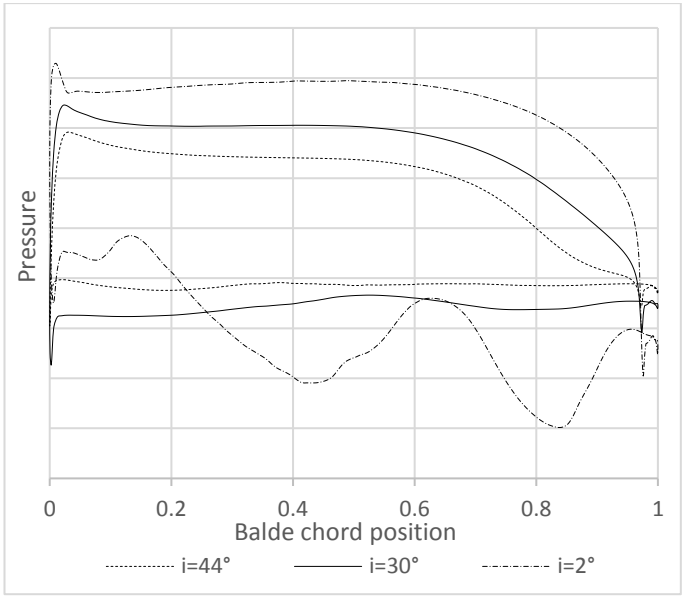

Figure 8 - Comparison of blade loading at 90% span

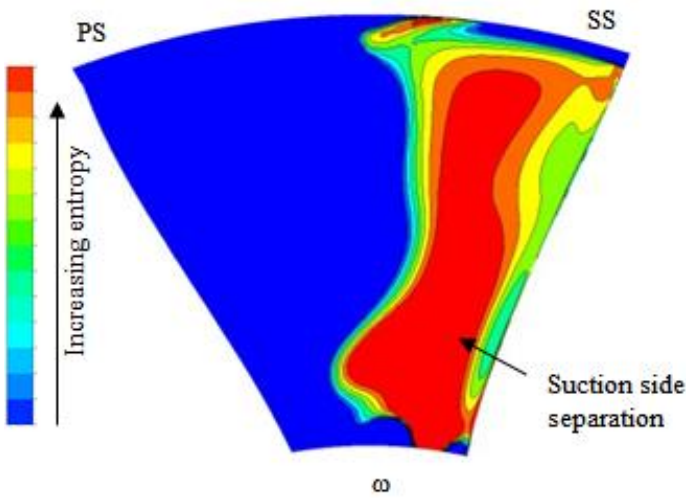

Figure 9 - Static entropy plot illustrating suction surface separation at 40% chord for i=44° case

At the design condition an incidence angle above +20° could not be produced as it required excessive tangential flow at rotor inlet. For the design condition the rotor was more tolerant to changes to the inlet flow conditions. Peak efficiency was achieved with an incidence angle of 5°. Three cases were selected for detailed comparison with incidence angles of i=18°, i=5° (optimum efficiency) and i=-31°. The spanwise distribution of incidence angle across the leading edge for each case is provided in Figure 10. The i=5° case achieved favourable incidence above 40% span and thus little flow separation in this region. However, below 40% span the positive incidence produced a large region of flow separation, as illustrated in Figure 11. The separation travelled up the blade suction surface towards the shroud as it moved downstream, before combining with the tip leakage flow. The i=-31° case experienced only a minor region of flow separation on the suction surface which was confined to a region close to the hub. Close to the mid-span of the i=-31° case the flow became excessively negative, causing a small separation from the pressure surface. The i=-31° case experienced the highest tip leakage losses, due in part to the greater blade loading close to the shroud. The greater blade loading produced a stronger trailing edge wake in the i=-31° case, further compromising rotor efficiency. The i=18° case operated with similar flow conditions to the i=5° case, however the leading edge separation was greater, particularly towards the hub. An illustration of the entropy generation at 50% chord is provided in Figure 11, where the large tip leakage losses in the i=-31° case and hub side separation in the i=5° and i=18° cases can be observed.

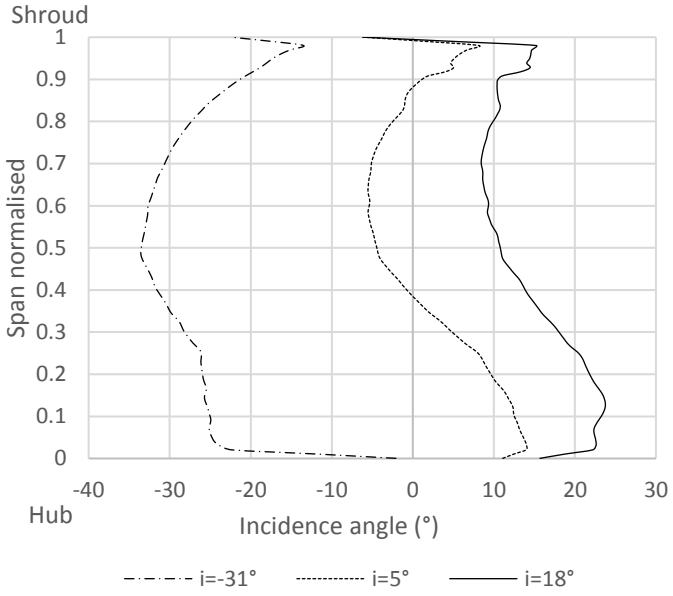

Figure 10 - Spanwise distribution of incidence angle for design condition cases

From examining the turbine at both design and off-design operation, it is evident that modifying the absolute inlet flow angle to control the incidence angle has a substantial impact on the flow features within the rotor passage, extending beyond the extent of the leading edge separation. In agreement with the published literature, shifting turbine operation towards negative incidence was found to minimise leading edge separation. However, the degree of reaction across the rotor and blade loading increased. This produced greater tip leakage flow and trailing edge wake. Therefore peak efficiency was produced when the best compromise between competing loss factors was achieved. As the disadvantages of positive incidence were greatest at the hub, and the negative effects of high blade loading greatest at the shroud, it was considered that the turbine performance may benefit from varying the spanwise distribution of inlet flow angle to control the variation of incidence angle across the leading edge.

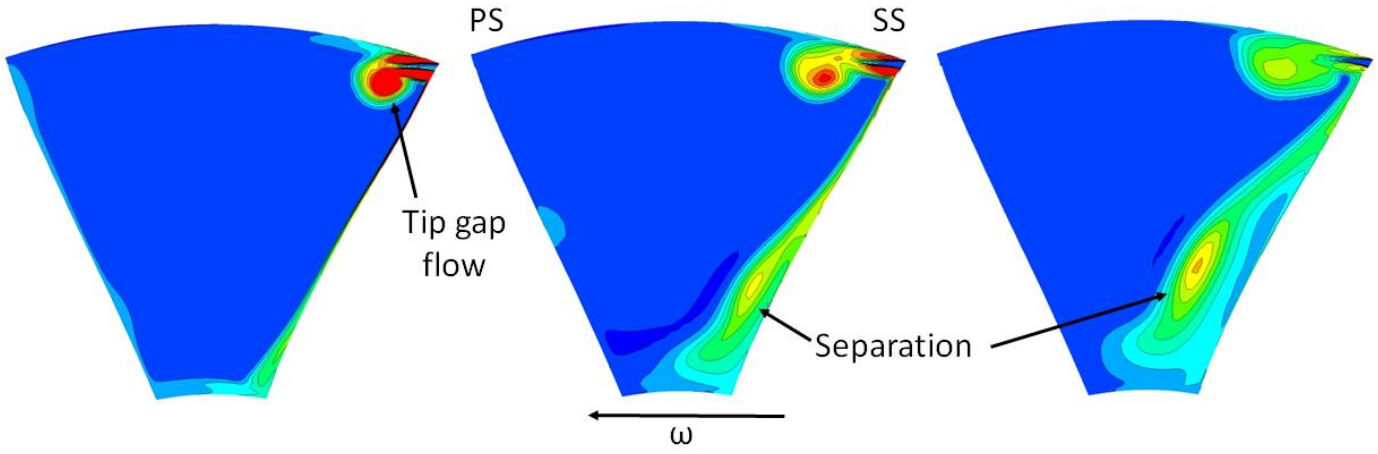

Figure 11 - Static entropy plots for spanwise variation of flow angle cases, i=-31° (left), i=+5 (middle) and i=+18° (right) at 50% chord length

4.2 Spanwise variation of flow angle

The results from section 4.1 indicated that the MFT experienced a variation of incidence across the leading edge. The effects of minimising the separation were examined by simulating the turbine with a range of different flow angle distributions between the hub and shroud. To ensure a fair comparison between cases, the average flow angle across the inlet was maintained constant. For this analysis the turbine was simulated at the same off-design condition considered in section 4.1. The peak efficiency point was selected which corresponded to an average stationary frame inlet flow angle of 70° and i = 30°.

The results from varying flow angle distribution are presented in Figure 12, where a positive variation represents an increased absolute flow angle towards the shroud and a decrease towards the hub, and a negative angle represents a decrease in absolute flow angle towards the shroud and an increase towards the hub. All cases had comparable mass flow rates and degree of reaction. The results indicated that a low flow angle at the hub and a large angle at the shroud improved the efficiency by up to 1% above the normalised baseline. For the opposite flow distributions, with larger flow angles towards the hub, a significant drop in efficiency was observed. A detailed comparison was conducted between the baseline case and cases with variations of +7° and -7°. The +7° case achieved a 1% efficiency improvement and the -7° case a 1.9% efficiency reduction. The incidence angle distributions achieved across the leading edge of the three cases are provided in
Figure 15. The decrease in radius across the leading edge produced a more positive incidence angle towards the hub in the baseline case. However, the reduction in flow angle towards the hub for +7° case was sufficient to counteract the effect of decreasing radius. The -7° case experienced severe positive incidence near the hub and a minor improvement in incidence angle close to the shroud. The different incidence angle distributions impacted the formation of flow features downstream of the leading edge. A comparison of the passage entropy at 25% chord position is illustrated in Figure 13. The reduced incidence close to the hub for the +7° case resulted in only minor separation for this region.

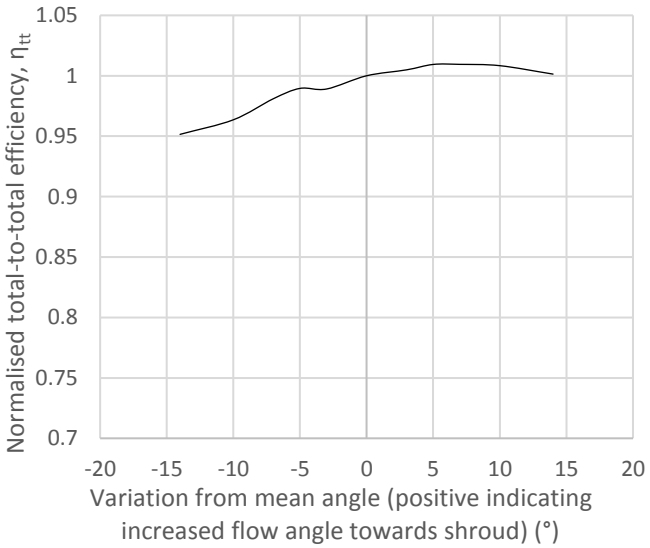

Figure 12 - Normalised efficiency vs variation in inlet flow angle for off-design operation

The drawback of this approach was a larger region of separation close to the shroud, due to the positive incidence in this region. In addition to varying the incidence angle, altering the inlet flow angle also impacted the mass flow distribution across the inlet, as a result of the change in radial velocity and the condition of uniform total pressure. This factor resulted in a greater mass flow rate towards the hub, and lower mass flow rate towards the shroud for the +7° case. This proved beneficial as a greater portion of the flow was in the low loss region close to the hub and only a small flow rate was present close to the shroud. This lessened the impact of the increased shroud separation. For the -7° case, the separation region close to the hub increased compared to the baseline, as a result of the highly positive incidence angle.

The suction surface separation immediately following the leading edge at the shroud was reduced, due to the improved incidence angle. However downstream of this point it increased in size and little advantage was gained compared to the baseline case.

Downstream of the initial flow separation region the tip leakage vortex became the driving loss factor. For the +7° case the lower mass flow at the shroud reduced the impact of the positive incidence angle on the tip gap flow. This resulted in lower tip leakage loss and reduced entropy generation in the rotor passage. A comparison of entropy generation at 95% chord position is provided in Figure 14. For the -7° case the higher mass flow towards the shroud increased the tip gap flow and the associated passage loss. Although the size of the tip leakage vortex decreased slightly for the -7° case, the greater mass flow in this region increased the overall loss. For the +7° case, the reduction in tip leakage vortex size was further benefited by a lower mass flow rate in this region. These factors resulted in the +7° case experiencing a 2.7% reduction in static entropy at the exit of the rotor passage and the -7° case experiencing a 4.5% increase, compared to the baseline.

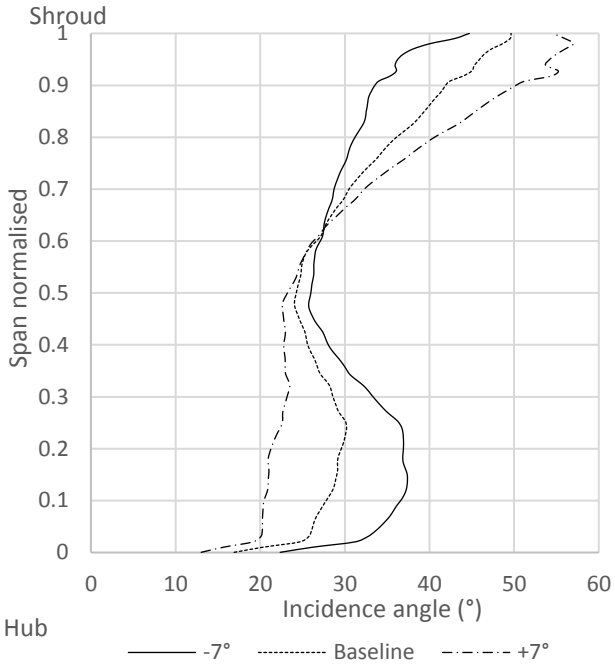

Figure 15 - Achieved spanwise distribution of incidence angle for varying inlet flow angle distributions

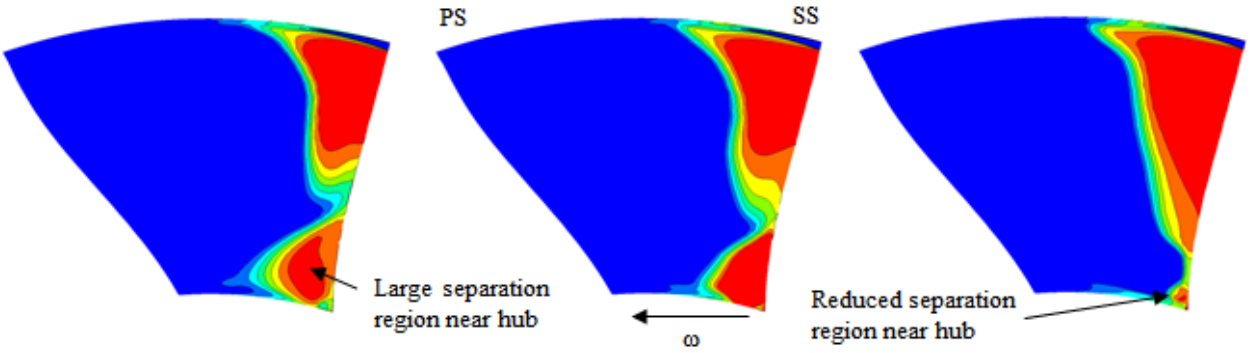

Figure 13 - Static entropy plots for spanwise variation of flow angle cases, -7° (left), baseline (middle) and +7° (right) at 25% chord length

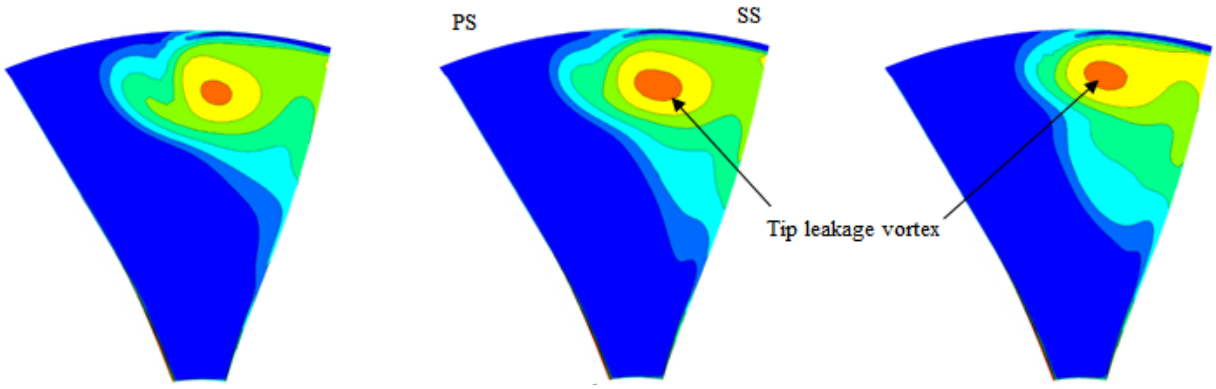

Figure 14 - Static entropy plots for spanwise variation of flow angle cases, -7° (left), baseline (middle) and +7° (right) at 95% chord length

4.3 Effects of inlet flow cone angle

The distinguishing feature of a MFT is that it has both axial and radial flow components at rotor inlet, resulting in a non-90° flow cone angle. To examine the effect of the flow cone angle on rotor performance, the turbine was simulated for flow cone angles between 45° (positive axial flow velocity) and 135° (negative axial flow velocity), as defined in Figure 1. The rotor was first examined at the design condition with a nominal incidence angle of 5°. At this point the flow cone angle was found to have limited impact on performance between λ=87° and λ=98°. At larger flow cone angles the performance decreased by up to 0.6% at λ=120°. For flow angles below the optimum, turbine performance decreased significantly dropping by 5.4% for the λ=45° case. For the off-design analysis a nominal incidence angle of 34° was selected, corresponding to high efficiency for this point. A comparison of flow cone angle against efficiency is provided in Figure 16. Cases with inlet flow cone angles of λ=65°, λ=90° (baseline) and λ=95° were selected for detailed comparison. The λ=95° case had the highest efficiency, with a 0.6% increase over the baseline. This indicated that a minor negative axial velocity at rotor inlet was desirable. The results indicated that a flow cone angle below 90° could negatively impact turbine performance at this off-design condition. The 65° case experienced a 1.5% decrease in efficiency compared to the baseline. After the rotor inlet the flow turned with the passage, altering the flow cone angle between the inlet and leading edge, resulting in flow cone angles at the leading edge of 58.6°, 63.8° and 64.6° for λ=65°, λ=90° and λ=95° cases, respectively.

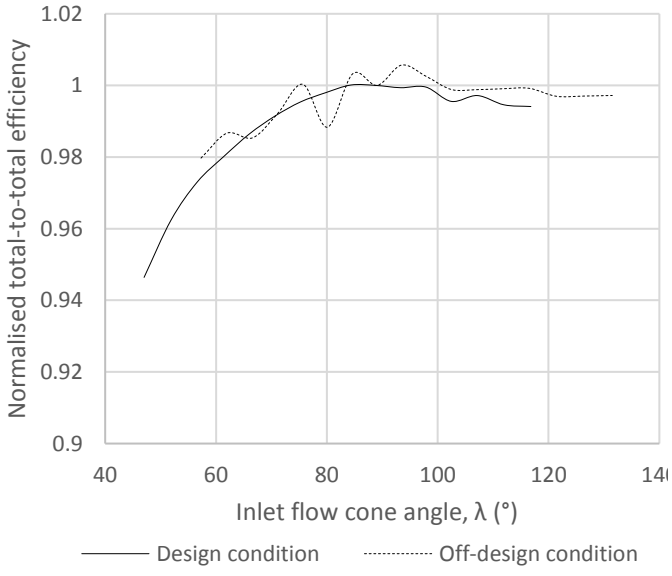

Figure 16 - Variation of normalised total-to-total efficiency with inlet flow cone angle

An examination for the flow fields within the rotor passage revealed that at the leading edge, the minor axial velocity in the λ=95° case had biased the inlet flow towards the hub, increasing the mass flow rate in this region. Whereas for the λ=65° case the flow was directed primarily towards the shroud. The significant change in spanwise distribution of mass flow between the cases is illustrated in Figure 17, with the values normalised against the average mass flow. Due the requirement of uniform inlet total pressure, an increase in mass flow rate corresponded in an increase in the radial velocity component. As the circumferential velocity component remained relatively unaffected by flow cone angle, different incidence angle distributions were produced for each case. For the three cases analysed, the incidence angle distributions are presented in Figure 18.

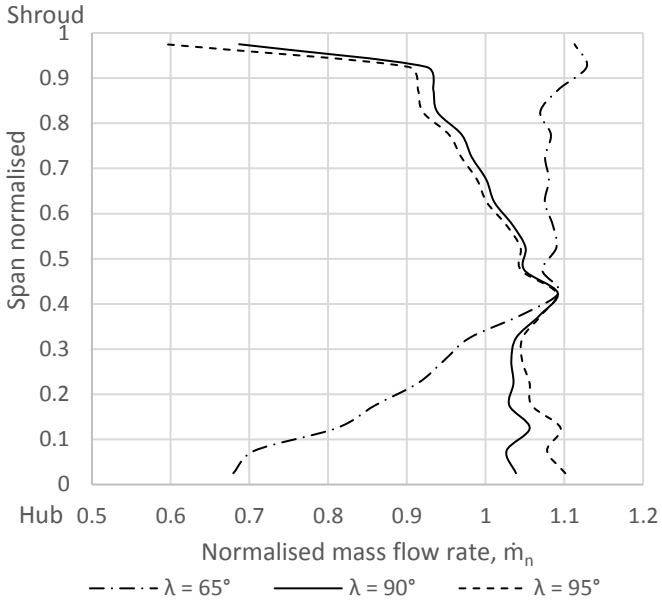

Figure 17 - Spanwise distribution of mass flow, normalised against mean mass flow

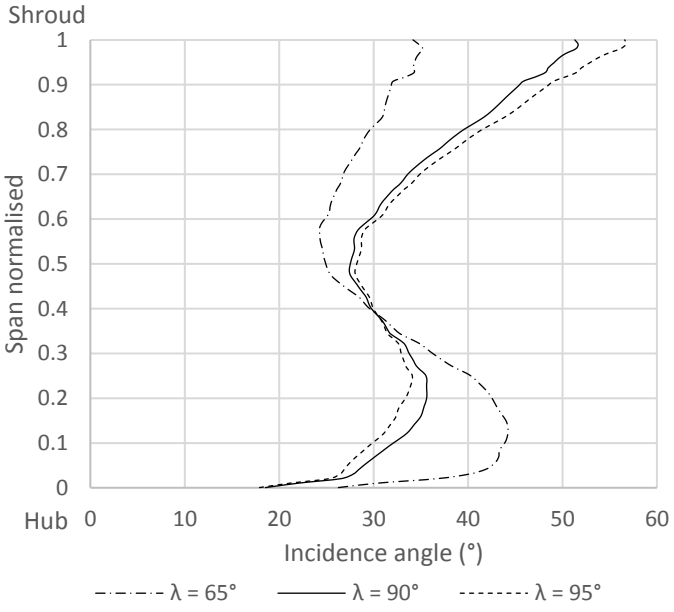

Figure 18 - Spanwise distribution of incidence angle for inlet cone angle comparison

This investigation found that a lower incidence angle at the hub and a positive angle at the shroud, improved turbine efficiency. This agrees with the conclusions of section 4.2. The improved efficiency was contributed to reduced flow separation and increased mass flow rate close to the hub. As the flow cone angle increased above 90° the extent of flow turning in the meridional plane near the shroud increased, resulting in a separation from the shroud wall forming at large flow cone angles. Although the turning disrupted the flow field and generated additional loss, it provided a benefit by reducing the mass flow rate in the high loss region close to the shroud. Lower flow cone angles, below 90°, produced an increased flow rate towards the shroud due to the positive axial flow component. This drove greater tip leakage loss and increased entropy generation, lowering turbine efficiency. An overview of rotor passage entropy is provided in Figure 19.

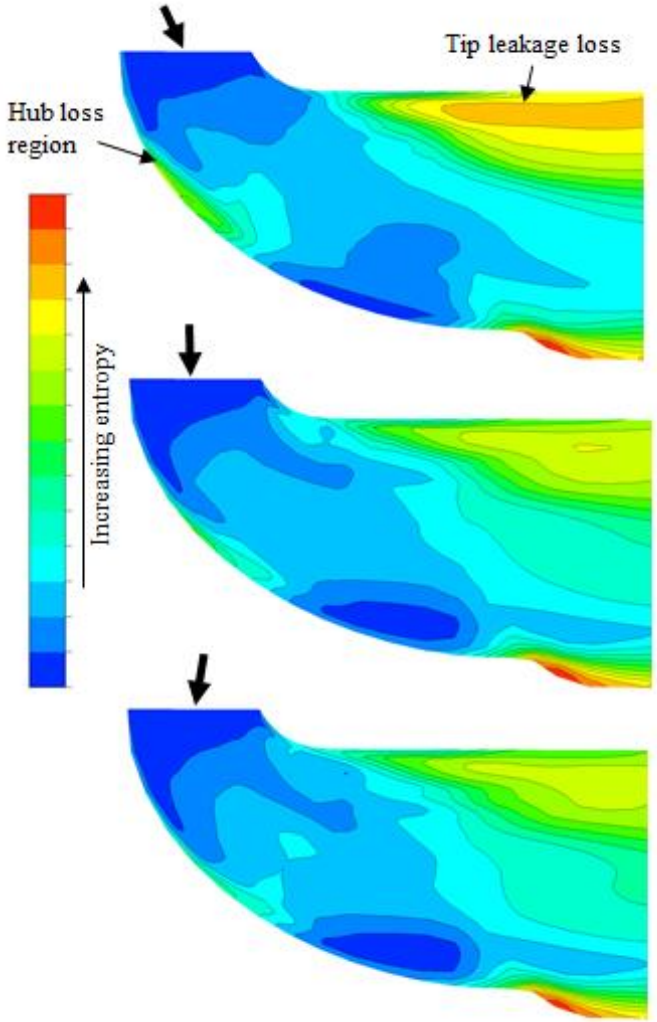

Figure 19 - Meridional plot of static entropy for λ=65° (top), λ=90° (middle) and λ=95° (bottom) cases

It can be observed that for the λ=65° case a region of high entropy existed close to the hub side of the leading edge, this corresponded to the shroud suction surface separation. The impact of this loss was reduced by low mass flow rate at this span location, as illustrated in Figure 17. At this location, the λ=90° case experienced only a minor increase in entropy and the region was almost non-existent in the λ=95° case. The increase in loss due to tip gap flow for λ=65° case is also evident in Figure 19, as a large region of loss exists close to the shroud, which is significantly smaller in the other cases. The changes in flow cone angle were found to have limited impact on the size and intensity of the trailing edge wake. Therefore, it has been determined that a clear advantage can be obtained by optimising the flow cone angle to bias the inlet flow towards the hub, to improve incidence angle and reduce the tip leakage flow.

5. Conclusions

Presented is a comparison of the effects of inlet flow angle, spanwise distribution of inlet flow angle and flow cone angle for a mixed flow turbine. From the study it is evident that the optimum incidence angle is dependent on the turbine operating condition. In agreement with the existing literature, leading edge separation was minimised for a minor negative incidence angle, however the optimum incidence angle range was not as negative as would be required for an equivalent RFT. However for a given rotor geometry, creating a negative incidence angle required a small absolute inlet flow angle, which increased the degree of reaction across the rotor. Higher blade loading in the cases with smaller inlet flow angles generated greater tip leakage flow and trailing edge wake. Optimum efficiency is therefore obtained by achieving the best compromise between competing loss factors, including leading edge separation and in particular the significant separation close to the hub, tip leaking flow and trailing edge wake.

To attempt to minimise the different loss regions in the rotor passage, the inlet flow angle was varied between the hub and shroud. At the off-design condition considered in this study, rotor performance was improved by reducing the absolute flow angle towards the hub and increasing it at the shroud. This reduced the large flow separation close to the hub and directed a greater proportion of flow towards the hub region, while lowering the flow rate towards the high loss region near the shroud. By adopting this approach the MFT efficiency was increased by 1% above the uniform flow angle baseline case. The results also indicated that inlet flow conditions that resulted in large flow angles at the hub and a lower flow angle at the shroud significantly reduced turbine performance, reducing efficiency by 5% for a flow angle variation of 14° from the mean angle. It is therefore important to ensure that such flow conditions are avoided.

By including a flow cone angle of 95° an improvement in turbine efficiency of 0.6% was achieved at off-design operation compared to the baseline. As with the spanwise variation of flow angle, this was the result of improved incidence close to the hub and a greater proportion of mass flow towards this region. This combined with lower mass flow towards the shroud, lowered the overall loss generation within the rotor passage.
The results have revealed that the distribution of flow angle across the inlet can be altered to reduce the suction side

separation close to the hub in a MFT. This provided a flow path with lower entropy generation. Additionally, by directing the flow away from the shroud and towards the hub, the low loss region close to the hub can be better utilised and the tip leakage flow reduced, improving overall turbine efficiency.

The work undertaken for this study forms part of an ongoing project on the topic. The study focused solely on examining the impact of different flow conditions, imposed at rotor inlet, on the performance of a MFT. The practicalities of producing such flow conditions were not considered as part of this study.

6. Acknowledgements

The authors would like to thank IHI Charging Systems International GmbH for their support of this work and ANSYS Inc. for the provision of their CFX software for use in this work

7. Nomenclature

h	Enthalpy
i	Incidence
$\dot{m}$	Mass Flow Rate
R	Degree of Reaction
β	Relative Flow Angle
β_b	Blade Angle
η_{tt}	Total-to-Total Efficiency
λ	Flow Cone Angle
Λ	Blade Cone Angle
φ	Blade Camber Angle
ω	Rotational Speed

A/R	Area Ratio
CFD	Computational Fluid Dynamics
MFT	Mixed Flow Turbine
PS	Pressure Side
QUB	Queens University Belfast
RFT	Radial Flow Turbine
RMS	Root Mean Square
SS	Suction Side
SST	Shear Stress Transport
U/C_s	Velocity Ratio

8. References

[1] V. A. W. Hillier and P. Coombes. Hillier's Fundamentals of Motor Vehicle Technology (5th ed.) 2004.

[2] R. Stone. Introduction to Internal Combustion Engines (4th ed.) 1999.

[3] D. Japikse and N. C. Baines. Introduction to Turbomachinery 1997.

[4] H. E. Rohlik, "Radial-inflow turbines," in Turbine Design and Application, Vol. 3 ed., A. J. Glassman, Ed. NASA SP 290, 1975, pp. 279--306.

[5] S. W. T. Spence and D. W. Artt An experimental assessment of incidence losses in a radial inflow turbine rotor. Proc. Instn Mech. Engrs, Part A, Journal of Power and Energy, 1998, 212 (1), 43-53. ISSN 0957 6509, [doi:10.1243/0957650981536727].

[6] H. Moustapha, M. F. Zelesky, N. C. Baines and D. Japikse. Axial and Radial Turbines 20032.

[7] J. R. Walkingshaw, S. W. T. Spence, J. Ehrhard, and D. Thornhill, 2011, An investigation into improving off-design performance in a turbocharger turbine utilizing non-radial blading, Paper No. GT2011-45717, Proceedings of ASME Turbo Expo 2011, Vancouver, 6-10 June, Vol. 7, pp. 2023-2032, doi: 10.1115/GT2011-45717.

[8] N. Watson and M. S. Janota, Turbocharging the Internal Combustion Engine. The MacMillan Press Ltd, 1982.

[9] B. Lüddecke, D. Filsinger and J. Ehrhard. On mixed flow turbines for automotive turbocharger applications. International Journal of Rotating Machinery 20122012.

[10] I. N. Merdes, D. C. Enderle, D. G. Vent and I. R. Weller. Der neue vierzylinderottomotor mit turboaufladung von mercedes-benz. MTZ-Motortechnische Zeitschrift 72(12), pp. 942-951. 2011.

[11] P. Lückert, F. Kreitmann, N. Merdes, R. Weller, A. Rehberger, K. Bruchner, K. Schwedler, H. Ottenbacher and T. Keller. The New 1.8-Litre 4-Cylinder Petrol Engine with Direct Injection and Turbocharging for all Passenger Cars with Standard Drivetrains from Mercedes-Benz 2009.

[12] D. Hagelstein, L. Hentschel, S. Strobel, R. Szengel, J. Theobald and H. Middendorf. Die aufladeentwicklung für den neuen 1.2 l TSI motor von volkswagen. Presented at 14th Aufladetechnische Konferenz, Dresden, Sept.. 2009.

[13] F. Bäumel, J. Jedro, C. Weber, A. Hinkelmann, A. Mayer and C. Kirschner. The turbocharger of the third generation of the AUDI R4-TFSI engines using the example of the new 1.8 l TFSI. Presented at 16th Supercharging Conference, Dresden, Sept. 2011.

[14] D. Palfreyman and R. F. Martinez-Botas. Numerical study of the internal flow field characteristics in mixed flow turbines. Presented at American Society of Mechanical

Engineers, International Gas Turbine Institute, Turbo Expo (Publication) IGTI. 2002.

[15] T. Leonard, S. W. T. Spence, J. Early, and D. Filsinger, 2014, A numerical study of inlet geometry for a low inertia mixed flow turbocharger turbine, Paper No. GT2014-25850, Proceedings of ASME Turbo Expo 2014, Dusseldorf, 16-20 June, Vol. 2D, doi:10.1115/GT2014-25850

[16] P. Walker and J. Hesketh. Design of low-reaction steam turbine blades. Proc. Inst. Mech. Eng. Part C 213(2), pp. 157-171. 1998.

[17] S. Havakechian and R. Greim. Aerodynamic design of 50 per cent reaction steam turbines. Proc. Inst. Mech. Eng. Part C 213(1), pp. 1-25. 1999.

[18] S. L. Dixon. Fluid Mechanics, Thermodynamics of Turbomachinery (5th , in SI/metric units ed.) 2005.

[19] J. R. Walkingshaw, S. W. T. Spence, D. Thornhill, and J. Ehrhard, 2010, A Numerical Study of the Flow Fields in a Highly Off-Design Variable Geometry Turbine. Paper No. GT2010-22669, Proceedings of ASME Turbo Expo 2010, Glasgow, 14-18 June, Vol. 7, pp. 1951-1960, doi: 10.1115/GT2010-22669.